Liquid film coating a fiber as a model system for the formation of bound states in active dispersive-dissipative nonlinear media

C. Duprat[1], F. Giorgiutti-Dauphiné[1], D. Tseluiko[2], S. Saprykin[2], and S. Kalliadasis[2]

[1]*CNRS, Univ Pierre et Marie Curie,*

Univ Paris-Sud, Lab FAST, Bat 502,

Campus Univ, Orsay 91405, France

[2]*Department of Chemical Engineering,*

Imperial College London, London SW7 2AZ, United Kingdom

(Dated: November 12, 2009)

Abstract

We analyze coherent-structures interaction and formation of bound states in active dispersive-dissipative nonlinear media using a viscous film coating a vertical fiber as a prototype. The coherent structures in this case are drop-like pulses that dominate the evolution of the film. We study experimentally the interaction dynamics and show evidence for formation of bound states. A theoretical explanation is provided through a coherent structures theory of a simple model for the flow.

1

Bound states, i.e., composites of two or more building blocks behaving as single objects, appear in a wide variety of physical settings, from atomic physics and quantum mechanics to biological physics and complex fluids [1]. In this Letter we demonstrate experimentally bound-state-formation phenomena in low-Reynolds-number interfacial hydrodynamics. Our experimental system consists of a viscous film flowing down a vertical fiber. The film is always unstable and spontaneously breaks up into a drop-like wavetrain [2]. Streamwise viscous diffusion plays a dispersive role that dramatically affects the wave selection, speeds, and shapes [3]. This system is a simple example of a nonlinear medium with energy supply, energy dissipation, and dispersion and as such it can be used as a prototype for the study of generic features of the pattern-formation dynamics of open-flow hydrodynamic and other systems. For example, the instability can be either absolute or convective [3]. In the latter case the interface is dominated by drop-like interacting pulses. We demonstrate that for sufficiently strong dispersion such pulses can form bound states.

A qualitative theoretical explanation of the observed bound-state-formation phenomena is provided with a coherent-structures theory for the generalized Kuramoto–Sivashinsky (gKS) equation. This equation has been postulated in the literature as a prototype for the study of pattern-formation dynamics and spatio-temporal complexity in active dispersive-dissipative media. For sufficiently small dispersion, it exhibits spatio-temporal chaos while sufficiently large dispersion "regularizes" the solution in favor of a train of solitary pulses which continuously interact with each other [4]. Such "dissipative solitons", as they are referred to by Christov and Velarde [4], are due to a precise balance between nonlinearity, energy supply at long wavelengths, and energy dissipation at short ones and they appear in many different contexts [5]. Coherent-structures theories have been formulated based on the idea of weak interaction between neighboring structures, e.g., Ref. [6]. For the gKS equation previous efforts [7] appear to have overlooked important details, in particular in relation to the spectra of the operators of the linearized system around the pulses and their adjoints. We offer for the first time a rigorous analysis of the spectra these operators and provide precise criteria for the existence of bound states of pulses of the gKS equation.

A sketch of the experimental set-up is shown in Fig. 1(a). Rhodorsil silicon oil v50 (density $\rho = 963 \, \text{kg/m}^3$, dynamic viscosity $\mu = 48 \times 10^{-3} \, \text{Pa s}$, surface tension $\gamma = 20.8 \times 10^{-3} \, \text{N/m}$, capillary length $\kappa^{-1} = 1.5$ mm at 25° C) flows on vertical Nylon fibers of 1.5 m length. Notations are shown in Fig. 1(b). x denotes the streamwise direction along the fiber. To
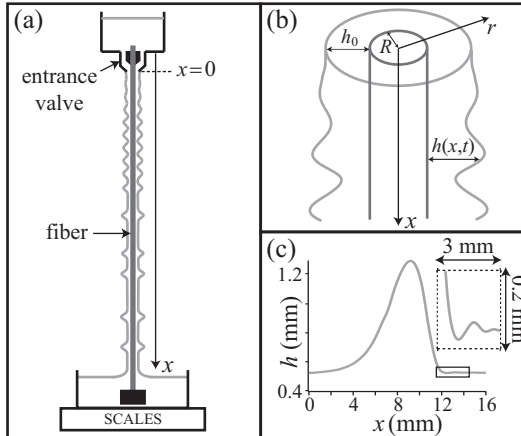
2

FIG. 1: (a) experimental set-up; (b) notations; (c) typical solitary-pulse shape ($R = 0.45$ mm).

ensure strong curvature effects, radii R are chosen to be small compared to the capillary length, 0.2 mm $< R <$ 0.475 mm, i.e., $R/\kappa^{-1} < 0.32$. A balance between viscous drag and gravity gives a characteristic speed $U_0 = \rho g h_0^2/2\mu$. The relevant dimensionless groups are the Reynolds number $Re = \rho U_0 h_0/\mu$ and the Weber number $We = \gamma/\rho U_0^2 h_0$. Parameters are chosen so that both surface tension and viscosity effects are important, i.e., 0.6 mm $< h_0 <$ 0.95 mm giving 3.5 cm/s $< U_0 <$ 8.8 cm/s, $30 > We > 3$, and $0.4 < Re < 1.7$.

The initially flat film breaks up into a regular drop-like train of coherent structures each of which resembles the pulse shown in Fig. 1(c). This instability results primarily from the capillary pressure induced by the azimuthal curvature (Rayleigh–Plateau instability); the pressure induced by the axial curvature has a stabilizing effect. Here we focus on the regime where the Rayleigh–Plateau instability competes with the viscous dispersive effect.

Spatio-temporal diagrams are obtained with a linear camera. The noise-driven dynamics is depicted in Fig. 2. The primary quasi-regular wavetrain is destabilized by numerous coalescence and capillary drainage enhanced events leading to the formation of saturated pulses, see Fig. 2(a). After a certain distance, typically 80 cm, no more coalescence occurs and the saturated pulses rearrange themselves through attractions and repulsions, see Fig. 2(b), **A** and **B**, respectively. Visualization of these events is obtained with a fast digital camera, see Fig. 2(c) and (d), respectively. During attraction (repulsion) the upstream pulse **1** accelerates (decelerates) while the downstream pulse **2** decelerates (accelerates). The pulses then lock on at a given distance, which remains constant, and both travel at constant speed forming a bound state. Although no obvious regular pattern is observed down the fiber,
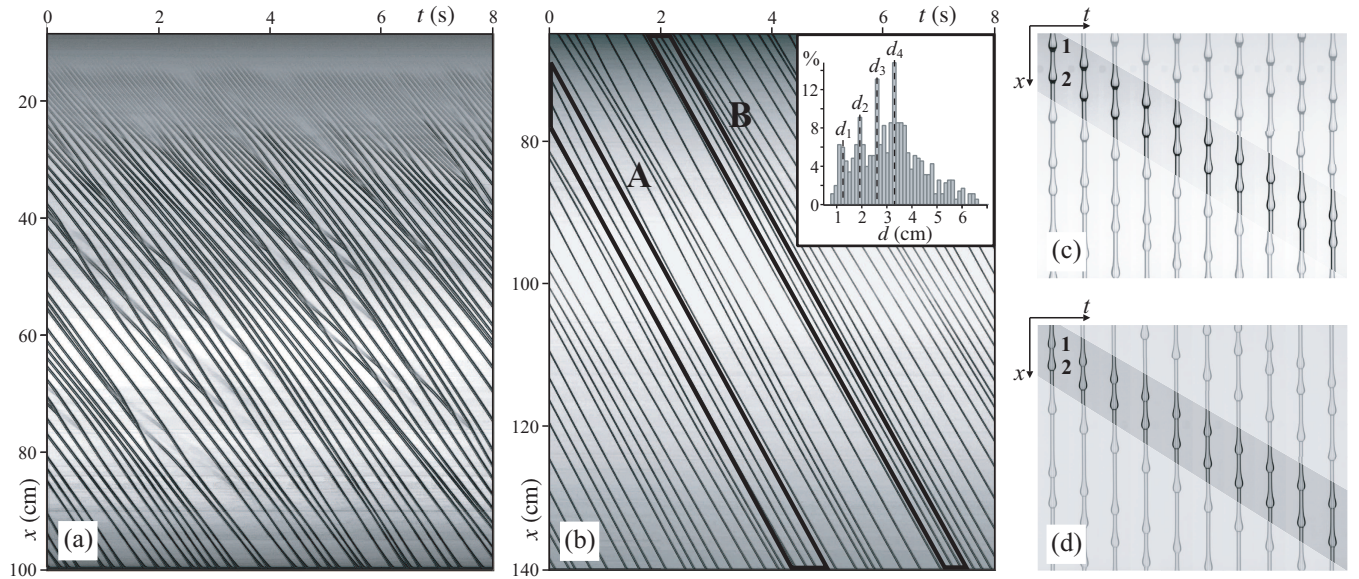
3

FIG. 2: Experimentally obtained world lines tracking the wave peaks during noise-driven evolution for $R = 0.45$ mm, $We = 18$, $Re = 0.56$, $\delta = 0.4$: (a) $0.07\,\text{m} < x < 1\,\text{m}$ and (b) $0.65\,\text{m} < x < 1.4\,\text{m}$; insert: histogram of the distances between pulses at the bottom of the fiber, $1.2\,\text{m} < x < 1.4\,\text{m}$. (c) and (d) show consecutive images (height: 9 cm) demonstrating attraction ($We = 5$, $Re = 1.2$, $\delta = 0.39$) and repulsion ($We = 3.4$, $Re = 1.5$, $\delta = 0.42$), respectively, for $R = 0.35$ mm. Time between two consecutive images is 0.08 s.

statistics on the separation distances between successive pulses performed at the bottom of the fiber (at around $x = 1.4$ m) and with a large ensemble averaging reveals a clear reorganization of the system with certain distances being selected. Indeed, in the histogram presented in Fig. 2(b), we observe that, although the distribution of distances is broad, four specific distances stand out, $d_1 \approx 1.2$ cm, $d_2 \approx 1.8$ cm, $d_3 \approx 2.6$ cm, and $d_4 \approx 3.35$ cm. The system appears to be heading towards organization. We have explored the parameter space by changing the fiber radius and the initial film thickness. Bound states are always observed with two to four preferred distances. Pulse rearrangement seems to be mainly promoted by interaction without substantial mass exchange. Waves then only interact through their tails whose specific structure is responsible for the observed phenomena. The characteristic profile of the waves is shown in Fig. 1(c). Surface tension and inertia lead to the front capillary ripples while viscous friction suppresses them. The steepening of the front is a nonlinear kinematic effect while inertia, gravity, and viscous drag are responsible for

4

the gentle monotonically increasing back edge. As two nearly identical pulses approach each other, the back slope of the downstream pulse **2** overlaps with a minimum (maximum) of one of the periodic capillary waves preceding the upstream pulse **1**. This generates a negative (positive) differential capillary pressure in the liquid ($\Delta p \sim -\gamma\, h_{xx}$) that drains fluid from **2** to **1** (**1** to **2**). This depresses (elevates) the back slope of the front pulse **2** and increases (decreases) its curvature. The generated differential capillary pressure then drains a small amount of fluid out of (into) the crest of **2**, slightly changing its amplitude and its speed, while the back pulse **1** experiences an opposite change in amplitude. The front pulse then moves slightly slower (faster) than the back pulse, and the pulses attract (repel) each other, see Fig. 2(c) and (d). This mechanism implies not only the existence of several possible distances between pulses but also that the distances between the neighboring prominent peaks in the histogram of Fig. 2(b) are roughly the same, i.e., $d_2 - d_1 \approx d_3 - d_2 \approx d_4 - d_3$, and are related to the period of the oscillations of the front tail of the pulse. An explanation for this effect is given below.

We start by deriving a simple model for the flow. The governing equations are the Navier–Stokes in cylindrical coordinates with the wall and the free-surface boundary conditions. We assume $R/h_0 = O(\epsilon^{-1})$, $We = O(\epsilon^{-2})$ and $Re = O(\epsilon)$, where $\epsilon \ll 1$ is the long-wave/film parameter, e.g., Ref. [8]. Through a weakly nonlinear expansion in which the amplitude deviation from h_0 is taken of $O(\epsilon^2)$, we obtain the following equation:

$$H_T - c_\delta H_X + H H_X + H_{XX} + \delta H_{XXX} + H_{XXXX} = 0, \tag{1}$$

already in a frame moving with the velocity of a pulse. X, T, and H are defined through

$$x = h_0 A^{-1/2}(X + c_\delta T) + 3B[2 + \tfrac{2}{3}\alpha - \tfrac{1}{2}\alpha^2]T, \tag{2a}$$

$$t = 3U_0^{-1}BT, \quad H = 12A^{1/2}Bh_0^{-2}(h - h_0), \tag{2b}$$

where $A = 8/5We + \alpha^2$, $B = h_0/WeReA^2$, and $\alpha = h_0/R$. The second term in (2a) is due to a transformation into the frame moving with the velocity of an infinitesimal wave, which is necessary to remove the advective term appearing in the weakly nonlinear expansion. The additional transformation into the frame moving with the velocity of the pulse results in the term $c_\delta T$ in the first brackets in (2a).

Equation (1) is the so-called gKS equation. It is the simplest possible prototype that retains the fundamental elements of active-dissipative nonlinear media: the dominant nonlinear term ($H H_X$), instability (H_{XX}), stability (H_{XXXX}), and dispersion (δH_{XXX}), where

5

$\delta = 6/We \, Re \, A^{1/2}$. Let $H_0 = H_0(X)$ be a stationary pulse satisfying the steady version of (1). We assume that $H = \sum_{i=1}^{n} H_i + \hat{H}$, where $H_i(X, T) = H_0(X - X_i(T))$ is a quasi-stationary pulse located at $X_i(T)$, $i = 1, \ldots, n$, and $\hat{H}$ is an overlap function. We consider weak interaction assuming that $L_i \equiv X_{i+1} - X_i = \log \varepsilon + O(1)$ for $i = 1, \ldots, n-1$, where $\varepsilon \ll 1$, and that the velocities of the pulses, X_i', $i = 1, \ldots, n$, and the overlap function, $\hat{H}$, are of $O(\varepsilon)$. The linearized equation for $\hat{H}$ in the vicinity of the ith pulse takes the form

$$\hat{H}_T - X_i' H_{iX} = \mathcal{L}_i \hat{H} - \alpha_i (H_{i-1} H_i)_X - \beta_i (H_i H_{i+1})_X, \qquad (3)$$

where $\alpha_i = \beta_i = 1$ for $1 < i < n$, $\alpha_1 = \beta_n = 0$, $\alpha_n = \beta_1 = 1$. $\mathcal{L}_i$'s are linear operators defined by $\mathcal{L}_i F = c_\delta F_X - F_{XX} - \delta F_{XXX} - F_{XXXX} - (H_i F)_X$. The formal adjoint operators, $\mathcal{L}_i^*$'s, with respect to the inner product in $L_{\mathbb{C}}^2$, $\langle f, g \rangle = \int_{-\infty}^{+\infty} f \bar{g} \, dX$, are given by $\mathcal{L}_i^* F = -c_\delta F_X - F_{XX} + \delta F_{XXX} - F_{XXXX} + H_i F_X$. The aim now is to project the dynamics in the vicinity of the ith pulse onto the null space of $\mathcal{L}_i$ spanned by the translational mode H_{iX}. Our analysis reveals that the null space of $\mathcal{L}_i^*$ is spanned by a constant and a function Ψ^i tending exponentially to different constants as $X \to \pm\infty$. Therefore, zero is not in the point spectrum of $\mathcal{L}_i^*$ on an infinite interval. Projections onto the null space of $\mathcal{L}_i$ are made rigorously by choosing an appropriate weighted space, namely, $L_a^2 = \{f : e^{aX} f \in L_{\mathbb{C}}^2\}$, where a is a positive sufficiently small number, with the inner product $\langle f, g \rangle_a = \langle e^{aX} f, e^{aX} g \rangle$. Studying the spectrum of $\mathcal{L}_i$ in L_a^2 is equivalent to studying the spectrum of the operator defined by $\mathcal{L}_i^a f = e^{aX} \mathcal{L}_i (e^{-aX} f)$ in $L_{\mathbb{C}}^2$, see Ref. [9]. Zero becomes an isolated eigenvalue of both $\mathcal{L}_i^a$ and $\mathcal{L}_i^{a*}$ of algebraic and geometric multiplicity unity and projections can now be made in the usual way. Assuming that $\hat{H}$ is in the null spaces of the projections, we arrive at the following system describing the leading-order dynamics of the locations of the pulses:

$$X_i' = \alpha_i S_2(X_i - X_{i-1}) + \beta_i S_1(X_{i+1} - X_i); \, 1 \leq i \leq n, \qquad (4)$$

where $S_{1,2}(L) \equiv -\int_{-\infty}^{\infty} H_0(X + \frac{1}{2}L) H_0(X - \frac{1}{2}L) \Psi_X^0(X \pm \frac{1}{2}L) \, dX$. Thus, the position of the ith pulse is governed by its interaction with the oscillatory front of the upstream pulse $(i - 1)$, described by S_2, and with the monotonic tail of the downstream pulse $(i + 1)$, described by S_1. System (4) can be re-written in terms of the separation distances L_i's and its fixed points then give the bound states, e.g., for a bound state of two pulses we must have $S_1(L_1) = S_2(L_1)$. At the same time, $S_{1,2}$ represent the velocities of the 1st and of the 2nd pulse relative to c_δ, respectively. The graphs of S_1 and S_2 are shown in Fig. 3(a) for
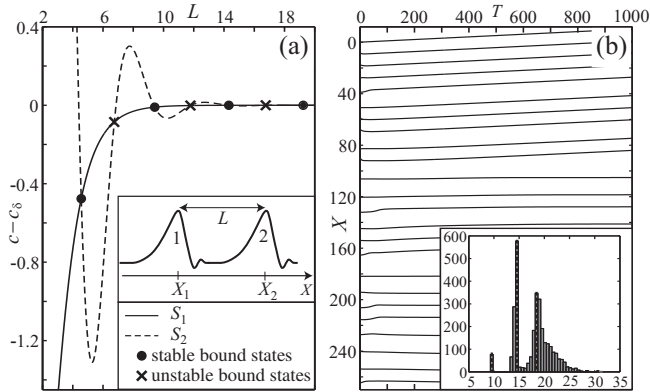
6

FIG. 3: (a) Dependence of S_1 and S_2 on the separation distance between two pulses for $\delta = 0.4$. (b) Evolution of pulses of the gKS equation for $\delta = 0.4$, in the frame of a solitary pulse obtained by solving (4). Subplot: histogram of the pulse separation distances (the initial distribution was taken to be normal with mean 18 and standard deviation 3).

$\delta = 0.4$. Depending on their initial separation distance L, pulses either attract ($S_1 > S_2$) or repel ($S_1 < S_2$) each other. As they get closer or further from each other, their velocity difference decreases until both pulses propagate at the same velocity, forming a bound state. The abscissas of the intersection points hence indicate the separation distances for which bound states can be formed. By analyzing the behavior of $S_{1,2}$ as $L \to \infty$, it can be shown that if $\delta < \delta^* \approx 0.85$, there is countable infinite number of intersections. Otherwise, the number is finite, but for $\delta \gtrsim 1.3$ there are no intersections (we note that for $\delta \gtrsim 1$, numerical experiments with the gKS equation show that we do not have formation of bound states).

We have solved numerically (4) for two pulses and $\delta = 0.4$ (as in Fig. 2(a) and (b)) and compared the results with numerical solutions of (1) when the initial condition is a superposition of two pulses with the same separation distance as that for (4). We found very good agreement between the two. Fig. 3(b) shows a typical solution of (4) and the world lines of 24 pulses. We observe both attractions and repulsions, formation of two- and three-pulse bound states while the world lines are similar to those obtained in our experiments and shown in Fig. 2(b). The subplot shows a histogram obtained from statistics on 3,000 pulse separation distances at $t = 1,000$. We observe three clear peaks formed at $\simeq 9.5$, 14, and 18.5, which are in very good agreement with the stable two-pulse bound state distances shown in Fig. 3(a) (the distance of $\simeq 4$ is disregarded as it corresponds to a two-hump pulse

which is never observed in the computations). The inset in Fig. 3(b) reveals a feature that is also present in the experiments (inset of Fig. 2(b)): the distances between the neighboring prominent peaks in the histograms are roughly the same. The theoretical explanation for this is in Fig. 3(a): S_2 is oscillatory approaching a sinusoidal function for $L \gtrsim 6$ while S_1 levels off quickly with L. Converting the dimensionless distances 9.5, 14, and 18.5 to dimensional ones, gives 0.42, 0.62, and 0.82 cm. When compared with the first three peaks occurring in the histogram in Fig. 2(b) at $d_1 \approx 1.2$ cm, $d_2 \approx 1.8$ cm, and $d_3 \approx 2.6$ cm, we find that the experimental distances are larger than the theoretical ones by a factor of $\simeq 3$. Hence, we have qualitative agreement, in that the system appears to select (via both attractions and repulsions) certain separation distances at large times (which are also of the same order with the experiments). However, we do not have quantitative agreement, but this is to be expected as for the theory R was assumed to be large compared to h_0, which is not the case in experiments, where $\alpha = O(1)$. Violation of this assumption affects significantly the constant A and, therefore, the rescaling of the distances. Smaller thicknesses are not reachable experimentally: below a critical film thickness of $\simeq 0.5$ mm, no flat film can emerge, instead dripping of the liquid from the faucet is observed. The requirement $\alpha \ll 1$ is approached on a larger radius fiber or with smaller thicknesses on smaller radii; however, under these conditions either $\delta \gtrsim 1$ and we do not observe the formation of bound states as noted earlier or $\delta \lesssim 0.1$ in which case the behavior is chaotic (we are close to the KS limit). Experimentally, bound states are observed for $0.1 \lesssim \delta \lesssim 1$, when both dispersive and dissipative effects are strong. This also implies that δ is indeed the right parameter to measure dispersive effects.

To conclude, we have examined experimentally pulse interaction and formation of bound states on the surface of a film coating a vertical fiber. Theoretical support for these phenomena was provided with a coherent structures theory for the gKS equation. This equation is not strictly speaking applicable for $\alpha = O(1)$, the regime in which the experiments were conducted, so that a quantitative agreement is not quite achieved. However, it is the simplest possible model for the physical system, containing all its important elements, and thus capable of describing the experiments qualitatively.

8

[1] L. E. Ballentine, *Quantum Mechanics: A Modern Development* (World Scientific, Singapore, 1998); K. Drescher, K. C. Leptos, I. Tuval, T. Ishikawa, T. J. Pedley, and R. E. Goldstein, Phys. Rev. Lett. **102**, 168101 (2009); G. A. Voth, B. Bigger, M. R. Buckley, W. Losert, M. P. Brenner, H. A. Stone, and J. P. Gollub, Phys. Rev. Lett. **88**, 234301 (2002).

[2] A. L. Frenkel, Europhys. Lett. **18**, 583 (1992); S. Kalliadasis and H.-C. Chang, J. Fluid Mech. **261**, 136 (1994).

[3] C. Duprat, C. Ruyer-Quil, S. Kalliadasis, and F. Giorgiutti-Dauphiné, Phys. Rev. Lett. **98**, 244502 (2007); C. Ruyer-Quil, P. Treveleyan, F. Giorgiutti-Dauphiné, C. Duprat, and S. Kalliadasis, J. Fluid Mech. **603**, 431 (2008); C. Duprat, C. Ruyer-Quil, and F. Giorgiutti-Dauphiné, Phys. Fluids **21**, 042109 (2009).

[4] T. Kawahara, Phys. Rev. Lett **51**, 381 (1983); C. M. Alfaro, R. D. Benguria, and M. C. Depassier, Physica D **61**, 1 (1992); C. I. Christov and M. G. Velarde, Physica D **86**, 323 (1995).

[5] N. Akhmediev and A. Ankiewicz (Eds.) *Dissipative Solitons: From Optics to Biology and Medicine* (Lect. Notes Phys. **751** (2008)).

[6] S.-I. Ei, J. Dyn. Differ. Equ. **14**, 85 (2002); B. Sandstede, in *Handbook of Dynamical Systems II*, edited by B. Fiedler, (North-Holland, Amsterdam, 2002), p. 983.

[7] C. Elphick, G. R. Ierley, O. Regev, and E. A. Spiegel, Phys. Rev. A **44**, 1110 (1991); S.-I. Ei and T. Ohta, Phys. Rev. E **50**, 4672 (1994); H.-C. Chang and E. A. Demekhin, *Complex Wave Dynamics on Thin Films* (Elsevier, Amsterdam, 2002).

[8] S. Kalliadasis and U. Thiele (Eds.) *Thin Films of Soft Matter* (Springer-Wien, CISM, 2007).

[9] R. L. Pego and M. I. Weinstein, Phil. Trans. R. Soc. Lond. A **340**, 47 (1992).